Comparison of finite volume schemes for the mean curvature flow level set equation

Angela Handlovičová*, Karol Mikula† and Tomáš Oberhuber‡

Abstract

We discuss two different semi-implicit numerical schemes based on the finite volume method for approximation of the regularised mean curvature flow level set equation. The first, CVS scheme, is based on co-volume strategy and nonlinear terms, given by absolute value of gradient, are evaluated on pixel sides using splitted diamond-cell approach [11, 7, 8, 2, 6]. In the second, EHM scheme, the absolute values of gradients are evlauated inside the pixels by the Stokes formula and the scheme is obtained by imposing the continuity of fluxes on pixel sides [4]. Results concerning numerical analysis of the schemes are presented and a comparison of these numerical approximations on several representative examples are discussed including performance in image filtering. On testing examples with exact solutions the schemes behave similarly in solution error, but the EHM scheme has higher precision in gradient error. Finite volume numerical schemes also perform better in the filtering of a strong salt & pepper noise as the results obtained using finite difference method [10].

Keywords: Regularised mean curvature flow level set equation, stability and convergence of numerical solution, image filtering, finite volume method

1 Introduction

The standard mean curvature flow level set equation with the initial condition and the boundary conditions has the following form:

$$u_t - |\nabla u| \mathrm{div}\left(\frac{\nabla u}{|\nabla u|}\right) = 0, \text{ a.e. } (x,t) \in \Omega \times (0,T), \tag{1}$$

$$u(x,0) = u_0(x), \text{ a.e. } x \in \Omega, \tag{2}$$

$$u(x,t) = 0, \text{ a.e. } (x,t) \in \partial\Omega \times \mathbb{R}_+, \tag{3}$$

where

$$\begin{aligned} &\Omega \text{ be a polyhedral open bounded connected subset of } \mathbb{R}^d, \text{ with } d \in \mathbb{N}, \\ &\text{and } \partial\Omega = \overline{\Omega} \setminus \Omega \text{ its boundary}, \nu \text{ is the outward normal unit vector to } \partial\Omega. \end{aligned} \tag{4}$$

The model (1)-(3) can be considered also with zero Neumann boundary condition.
We use two regularizations of equation to overcome the zero value in the denominator. According to [5], we consider the regularization of the form $f(|\nabla u|) = \sqrt{|\nabla u|^2 + a^2}$, for given real number $a > 0$, which is further modified in [4] by considering

$$f(|\nabla u|) = \min(\sqrt{|\nabla u|^2 + a^2}, b), \tag{5}$$

*Dep. of Mathematics, Slovak University of Technology, angela@math.sk
†Dep. of Mathematics, Slovak University of Technology, mikula@math.sk
‡Dep. of Mathematics, Czech Technical University in Prague, tomas.oberhuber@fjfi.cvut.cz

for given real numbers $0 < a \leq b$. The first part of (5) is the same as in the previous case and use of the additional bound b is in accordance with the image processing applications. Indeed, on discrete grids, the gradient norms are lower than $\frac{Q}{h}$, where Q is a quantisation parameter and h is the side length of a pixel.
Then we substitute the equation (1) with the regularized one:

$$u_t - f(|\nabla u|)\mathrm{div}\left(\frac{\nabla u}{f(|\nabla u|)}\right) = 0, \text{ a.e. } (x,t) \in \Omega \times (0,T). \tag{6}$$

Definition 1.1 (Weak solution of (6)-(2)-(3)) *Let Ω be as in (4), $u_0 \in H_0^1(\Omega)$. We say that u is a weak solution of (6)-(2)-(3) if, for all $T > 0$,*

1. *$u \in L^2(0,T;H_0^1(\Omega))$ and $u_t \in L^2(\Omega \times (0,T))$ (hence $u \in C^0(0,T;L^2(\Omega))$).*
2. *$u(\cdot,0) = u_0$*
3. *the following holds*

$$\int_0^T \int_\Omega \left(\frac{u_t(x,t)v(x,t)}{f(|\nabla u(x,t)|)} + \frac{\nabla u(x,t)\cdot\nabla v(x,t)}{f(|\nabla u(x,t)|)}\right)\mathrm{d}x\mathrm{d}t = 0, \quad \forall v \in L^2(0,T;H_0^1(\Omega)). \tag{7}$$

In this paper we compare the results obtained by two numerical schemes based on finite volume method. The first, CVS scheme, is based on co-volume strategy and nonlinear terms, given by absolute value of gradient, are evaluated in pixel sides using splitted diamond-cell approach [11, 7, 8, 2, 6]. In the second, EHM scheme, the absolute values of gradients are evlauated inside the pixels by the Stokes formula and the scheme is obtained by imposing the continuity of fluxes on pixel sides [4]. Our co-volume strategy motivated by [11] was first introduced in [7] and then improved by the splitted diamond cell approach in [8] for 2D and in [2] for 3D problems. The theoretical results on CVS scheme were obtained in [6]. The second numerical scheme was proposed in [4] recently. We present numerical experiments where the exact solution is known and we compare the results obtained by both schemes with respect to accuracy, experimental order of convergence and CPU time points of view. Further numerical experiments are dealing with image filtering, were we present also a comparison with the classical finite difference scheme by Osher and Sethian [10].

2 Numerical schemes

In order to construct the numerical scheme we choose a uniform discrete time step $\tau = \frac{T}{N}$ and replace the time derivative in (6) by the backward difference. The nonlinear terms of the equation are treated from the previous time step while the linear ones are considered on the current time level, this means semi-implicitness of the time discretization.

Semi-implicit in time discretization: *Let τ be given time step, and u^0 be a given initial level set function. Then, for $n = 1,\ldots,N$, we look for a function u^n, solution of the equation*

$$\frac{1}{f(|\nabla u^{n-1}|)}\frac{u^n - u^{n-1}}{\tau} = \nabla.\left(\frac{\nabla u^n}{f(|\nabla u^{n-1})|}\right). \tag{8}$$

In what follows we propose two diffrent fully discretized numerical schemes, both based on finite volume method.

2.1 Finite volume scheme based on co-volume strategy (CVS)

Let us introduce now the fully discrete scheme as in [7, 8, 2, 6]. In the image processing applications, a digital image is given on a structure of pixels with rectangular shape in general (red rectangles in Figure

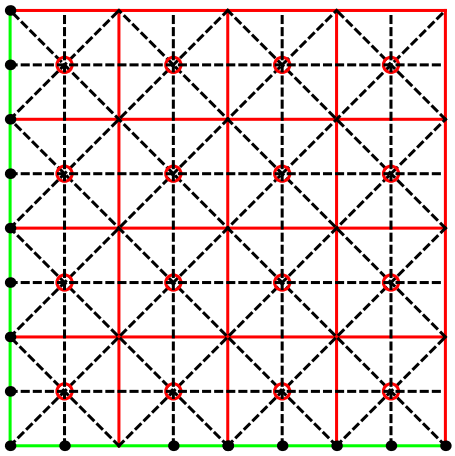

Figure 1: The co-volumes (red solid lines), the triangulation for the co-volume method (black dashed lines), and the degree of freedom (DF) nodes (red round points), the part of boundary $\partial\Omega$ (green lines) and the points where Dirichlet boundary condition is prescribed (black points).

1). We have to evaluate gradient of the level set function at the previous step $|\nabla u^{n-1}|$, so we put a triangulation (dashed black lines in Figure 1) onto the computational domain and then take a piecewise linear approximation of the level set function on this triangulation. Such approach will give a constant value of the gradient per triangle, allowing simple, fast and clear construction of fully-discrete system of equations. As can be seen in Figure 1, in our method the centers of pixels are connected by a new rectangular mesh and every new rectangle is splitted into four triangles. The centers of pixels will be called degree of freedom (DF) nodes. By this procedure we also get further nodes (at crossing of red lines in Figure 1) which, however, will not represent degrees of freedom. We will call them non-degree of freedom (NDF) nodes. Let a function u be given by discrete values in DF nodes. Then in additional NDF nodes we take the average value of the neighboring DF nodal values. By such defined values in NDF nodes, a piecewise linear approximation u_h of u on the triangulation can be built. For triangulation $\mathcal{T}_h$, given by the previous construction, we construct a complementary (dual) mesh. We modify a basic approach given in [11, 7] in such a way that our co-volume mesh will consist of cells p associated only with DF nodes p of $\mathcal{T}_h$, say $p = 1, \ldots, M$. Since there will be one-to-one correspondence between co-volumes and DF nodes, without any confusion, we use the same notation for them.
For each DF node p of $\mathcal{T}_h$, let $N(p)$ denote the set of all DF nodes q connected to the node p by an edge. We denote cardinality of this set by N_p. The edge connecting p and q will be denoted by σ_{pq} and its length by h_{pq}. Then every *co-volume* p is bounded by the lines (co-edges) e_{pq} that bisect and are perpendicular to the edges $\sigma_{pq}, q \in N(p)$. By this construction, the co-volume mesh corresponds exactly to the pixel structure of the image inside the computational domain Ω. We denote by $\mathcal{E}_{pq}$ the set of triangles having σ_{pq} as an edge. In a situation depicted in Figure 1, every $\mathcal{E}_{pq}$ consists of two triangles. For each $T \in \mathcal{E}_{pq}$ let c_{pq}^T be the length of the portion of e_{pq} that is in T, i.e., $c_{pq}^T = m(e_{pq} \cap T)$, where m is a measure in $I\!R^{d-1}$. Let $\mathcal{N}_p$ be the set of triangles that have DF node p as a vertex. Let u_h be a piecewise linear function on triangulation $\mathcal{T}_h$. We will denote a constant value of $|\nabla u_h|$ on $T \in \mathcal{T}_h$ by $|\nabla u_T|$. We will use the notation $u_p = u_h(x_p)$, where x_p is the coordinate of a (DF or NDF) node of triangulation $\mathcal{T}_h$, and also $u_p^n = u_{h,\tau}(x_p, t_n)$ where $u_{h,\tau}$ is our piecewise linear in space and time approximation of the solution to the regularized level set equation. Let u_h^0 be piecewise linear interpolation of the initial function u^0 on triangulation $\mathcal{T}_h$.
With these notations we are ready to derive the co-volume spatial discretization. As it is usual in finite volume methods, we integrate (6) over every co-volume p, $p = 1, \ldots, M$, and then using divergence

theorem we get an integral formulation of (6)

$$\int_p \frac{1}{|\nabla u^{n-1}|}\frac{u^n-u^{n-1}}{\tau}dx = \sum_{q\in N(p)}\int_{e_{pq}} \frac{1}{|\nabla u^{n-1}|}\frac{\partial u^n}{\partial \nu}ds \tag{9}$$

where ν is a unit outer normal to the boundary of p. Now using a piecewise linear reconstruction of u^{n-1} on triangulation $\mathcal{T}_h$ we get for the right hand side of (9)

$$\sum_{q\in N(p)}\left(\sum_{e_{pq}\in\mathcal{E}} c_{pq}^T \frac{1}{|\nabla u_T^{n-1}|}\right)\frac{u_q^n-u_p^n}{h_{pq}}. \tag{10}$$

For the left-hand side of (9) we use

$$m(p)\sum_{T\in\mathcal{N}_p}\frac{m(T\cap p)}{m(p)}\frac{1}{|\nabla u_T^{n-1}|}\frac{u_p^n-u_p^{n-1}}{\tau} \tag{11}$$

where $m(p)$ is a measure in $\mathbb{R}^d$ of co-volume p.
Let us restrict our considerations to uniform rectangular co-volumes with size length h, as plotted in Figure 1. Then $m(p)=h^2,\ m(e_{pq})=h_{pq}=h, c_{pq}^T=\frac{1}{2}m(e_{pq})$. We denote four neighbouring DF nodes of x_p by x_{q_1} (east), x_{q_2} (north), x_{q_3} (west), x_{q_4} (south), and the corners of co-volume p by x_{r_1} (top right), x_{r_2} (top left), x_{r_3} (bottom left), x_{r_4} (bottom right). The middle point of the edge e_{pq_i} is denoted by x_{m_i}, $i=1,\dots,4$.
Now we can define coefficients, where the ε-regularization (5) is taken into account, namely,

$$a_{pq}^{n-1} = \frac{1}{|\nabla u_{pq}^{n-1}|_\varepsilon} := \frac{1}{2}\left(\frac{1}{|\nabla u_{T_{pq}^1}^{n-1}|_\varepsilon}+\frac{1}{|\nabla u_{T_{pq}^2}^{n-1}|_\varepsilon}\right), \tag{12}$$

$$b_p^{n-1} := \frac{1}{|\nabla u_p^{n-1}|_\varepsilon} = \frac{1}{N_p}\sum_{q\in N(p)}\frac{1}{|\nabla u_{pq}^{n-1}|_\varepsilon}, \tag{13}$$

where $T_{pq}^1, T_{pq}^2 \in \mathcal{E}_{pq}$. For example for triangle with points x_p, x_{q_1}, x_{r_1} we have regularized gradient as in (5)

$$|\nabla u_{T_{pq_1}^1}^{n-1}|_\varepsilon = \min\left(\sqrt{\frac{(u_{q_1}-u_p)^2}{h^2}+\frac{(2(u_{r_1}-u_{m_1}))^2}{h^2}+\varepsilon^2}, b\right), \tag{14}$$

where the parameter b is an user defined parameter for the second regularization in (5) and it can be defined as $b=10^{10}$. Now our computational method can be written as follows.

Fully-discrete semi-implicit co-volume scheme: *Let $u_p^0,\ p=1,\dots,M$ be given discrete values of the initial condition. Then, for $n=1,\dots,N$ we look for $u_p^n, p=1,\dots,M$, satisfying*

$$b_p^{n-1}\ m(p)\ u_p^n + \tau\sum_{q\in N(p)} a_{pq}^{n-1} d_{pq}(u_p^n-u_q^n) = b_p^{n-1}\ m(p)\ u_p^{n-1}. \tag{15}$$

Remark 2.1 *The Dirichlet boundary conditions in CVS scheme are treated in such way, that we consider half triangles along the boundary $\partial\Omega$ (green lines in Figure 1) The gradients $|\nabla u_T^{n-1}|$ as well as normal derivatives in (10)- (14) and everywhere in T are evaluated using the values in the nodes of half triangles on the boundary $\partial\Omega$ (black points on green lines in Figure 1).*

Theoretical results for this scheme are based on the idea of G. Barles and P.E.Souganidis, where for converegence of the numerical scheme, the stability, consistency and monotonicity property must be fullfilled. Up till now, the convergence for proposed scheme is an open question, because of the lack of monotonicity property [1]. However, we have the following results, see [6].

Theorem: There exists unique solution $u_{h,\tau}$ of the numerical scheme for any value of the regularization parameter ε and for any h and τ. Moreover approximation scheme has **stability** and **consistency** property.

2.2 Finite volume scheme based on flux continuity and Stokes formula (EHM)

Definition 2.1 (Space discretisation) *Let Ω be as in* (4). A discretisation of Ω, denoted by $\mathcal{D}$, is defined as the triplet $\mathcal{D} = (\mathcal{M}, \mathcal{E}, \mathcal{P})$, where:

1. $\mathcal{M}$ is a finite family of nonempty connected open disjoint subsets of Ω (the "control volumes") such that $\overline{\Omega} = \cup_{p\in\mathcal{M}}\overline{p}$. For any $p \in \mathcal{M}$, let $\partial p = \overline{p} \setminus p$ be the boundary of p; let $|p| > 0$ denote the measure of p and let h_p denote the diameter of p and $h_{\mathcal{D}}$ denote the maximum value of $(h_p)_{p\in\mathcal{M}}$.

2. $\mathcal{E}$ is a finite family of disjoint subsets of $\overline{\Omega}$ (the "edges" of the mesh), such that, for all $\sigma \in \mathcal{E}$, σ is a nonempty open subset of a hyperplane of $\mathbb{R}^d$, whose $(d-1)$-dimensional measure $|\sigma|$ is strictly positive. We also assume that, for all $p \in \mathcal{M}$, there exists a subset $\mathcal{E}_p$ of $\mathcal{E}$ such that $\partial p = \cup_{\sigma\in\mathcal{E}_p}\overline{\sigma}$. For any $\sigma \in \mathcal{E}$, we denote by $\mathcal{M}_\sigma = \{p \in \mathcal{M}, \sigma \in \mathcal{E}_p\}$. We then assume that, for all $\sigma \in \mathcal{E}$, either $\mathcal{M}_\sigma$ has exactly one element and then $\sigma \subset \partial\Omega$ (the set of these interfaces, called boundary interfaces, is denoted by $\mathcal{E}_{\rm ext}$) or $\mathcal{M}_\sigma$ has exactly two elements (the set of these interfaces, called interior interfaces, is denoted by $\mathcal{E}_{\rm int}$). For all $\sigma \in \mathcal{E}$, we denote by x_σ the barycentre of σ. For all $p \in \mathcal{M}$ and $\sigma \in \mathcal{E}_p$, we denote by $\mathbf{n}_{p,\sigma}$ the unit vector normal to σ outward to p.

3. $\mathcal{P}$ is a family of points of Ω indexed by $\mathcal{M}$, denoted by $\mathcal{P} = (x_p)_{p\in\mathcal{M}}$, such that for all $p \in \mathcal{M}$, $x_p \in p$ and p is assumed to be x_p-star-shaped, which means that for all $x \in p$, the inclusion $[x_p, x] \subset p$ holds. Denoting by $d_{p\sigma}$ the Euclidean distance between x_p and the hyperplane including σ, one assumes that $d_{p\sigma} > 0$. We then denote by $D_{p,\sigma}$ the cone with vertex x_p and basis σ.

4. We make the important following assumption:

$$d_{p\sigma}\mathbf{n}_{p,\sigma} = x_\sigma - x_p,\ \forall p \in \mathcal{M},\ \forall \sigma \in \mathcal{E}_p. \tag{16}$$

Remark 2.2 *The preceding definition applies to triangular meshes if $d = 2$, with all angles acute, and to meshes build with orthogonal parallelepipedic control volumes (rectangles if $d = 2$).*

We denote

$$\theta_{\mathcal{D}} = \min_{p\in\mathcal{M}} \min_{\sigma\in\mathcal{E}_p} \frac{d_{p\sigma}}{h_p}. \tag{17}$$

Definition 2.2 (Space-time discretisation) *Let Ω be as in* (4) and let $T > 0$ be given. We say that $(\mathcal{D}, \tau)$ is a space-time discretisation of $\Omega\times(0,T)$ if $\mathcal{D}$ is a space discretisation of Ω in the sense of Definition 2.1 and if there exists $N_T \in \mathbb{N}$ with $T = (N_T + 1)\tau$.

Following the results from [4], where more general case of the problem is studied and both semi-implicit and fully implicit schemes are investigated, we present here just semi-implicit approach.
Let $(\mathcal{D}, \tau)$ be a space-time discretisation of $\Omega \times (0, T)$. We define the set $H_{\mathcal{D}} \subset \mathbb{R}^{\mathcal{M}} \times \mathbb{R}^{\mathcal{E}}$ such that $u_\sigma = 0$ for all $\sigma \in \mathcal{E}_{\rm ext}$. We define the following approximations of $|\nabla u|^2$ on $H_{\mathcal{D}}$:

$$N_p(u)^2 = \frac{1}{|p|}\sum_{\sigma\in\mathcal{E}_p} \frac{|\sigma|}{d_{p\sigma}}(u_\sigma - u_p)^2,\ \forall p \in \mathcal{M},\ \forall u \in H_{\mathcal{D}}. \tag{18}$$

The **semi-implicit scheme** is defined by

$$u_p^0 = \frac{1}{|p|}\int_p u_0(x)\mathrm{d}x,\ \forall p \in \mathcal{M}, \quad u_\sigma^0 = \frac{1}{|\sigma|}\int_\sigma u_0(x)\mathrm{d}s(x),\ \forall \sigma \in \mathcal{E}, \tag{19}$$

and the boundary condition is fulfilled thanks to

$$u_\sigma^{n+1} = 0,\ \forall \sigma \in \mathcal{E}_{\rm ext},\ \forall n \in \mathbb{N}. \tag{20}$$

Then in every new time step $t_{n+1} = (n+1)\tau$ we solve the system

$$\frac{|p|}{\tau\ f(N_p(u^n))}(u_p^{n+1} - u_p^n) - \frac{1}{f(N_p(u^n))}\sum_{\sigma\in\mathcal{E}_p}\frac{|\sigma|}{d_{p\sigma}}(u_\sigma^{n+1} - u_p^{n+1}) = 0, \quad \forall p \in \mathcal{M},\ \forall n \in \mathbb{N}, \tag{21}$$

where the following relation is given for the interior edges

$$\frac{u_\sigma^{n+1} - u_p^{n+1}}{f(N_p(u^n))\ d_{p\sigma}} + \frac{u_\sigma^{n+1} - u_q^{n+1}}{f(N_q(u^n))\ d_{q\sigma}} = 0,\ \forall \sigma \in \mathcal{E}_{\rm int} \text{ with } \mathcal{M}_\sigma = \{p,q\},\ \forall n \in \mathbb{N}. \tag{22}$$

By using the scheme we define the approximate solution $u_{\mathcal{D},\tau}$ in $\Omega \times \mathbb{R}_+$ by

$$u_{\mathcal{D},\tau}(x,0) = u_p^0,\ u_{\mathcal{D},\tau}(x,t) = u_p^{n+1},\ \text{for a.e. } x \in p,\ \forall t \in]n\tau,(n+1)\tau],\ \forall p \in \mathcal{M},\ \forall n \in \mathbb{N}. \tag{23}$$

We then define $N_{\mathcal{D},\tau}$by

$$\begin{array}{l} N_{\mathcal{D},\tau}(x,t) = N_p(u^n), \\ \text{for a.e. } x \in p, \quad \text{for a.e. } t \in]n\tau,(n+1)\tau[,\ \forall p \in \mathcal{M},\ \forall n \in \mathbb{N}. \end{array} \tag{24}$$

Finally, we define $\widehat{G}_{\mathcal{D},\tau}$ by

$$\begin{array}{l} \widehat{G}_{\mathcal{D},\tau}(x,t) = \dfrac{1}{|p|}\displaystyle\sum_{\sigma\in\mathcal{E}_p}|\sigma|(u_\sigma^{n+1} - u_p^{n+1})\mathbf{n}_{p\sigma}, \\ \text{for a.e. } x \in p, \quad \text{for a.e. } t \in]n\tau,(n+1)\tau[,\ \forall p \in \mathcal{M},\ \forall n \in \mathbb{N}. \end{array} \tag{25}$$

Let us denote by (HC) the following hypotheses:

- Ω is as in (4),
- $u_0 \in H_0^1(\Omega)$,
- The sequence $(\mathcal{D}_m,\tau_m)_{m\in\mathbb{N}}$ denotes a sequence of space-time discretisations of $\Omega \times (0,T)$ in the sense of Definition 2.2 such that $h_{\mathcal{D}_m}$ and $\tau_m > 0$ tends to 0 as $m \longrightarrow \infty$.
- There exists some $\theta > 0$ with $\theta < \theta_{\mathcal{D}_m}$ for all $m \in \mathbb{N}$, where $\theta_{\mathcal{D}}$ is defined by (17).
- For all $m \in \mathbb{N}$, the family $(u_p^n)_{p\in\mathcal{M},n\in\mathbb{N}}$ is such that (19), (20) and (21), (22) hold and the function $u_{\mathcal{D}_m,\tau_m}$ is defined by (23).

Then it holds [4]:

Theorem 2.1 *Let Hypotheses* (HC) *be fulfilled. We assume that the sequence $(\mathcal{D}_m,\tau_m)_{m\in\mathbb{N}}$ denotes an extracted sub-sequence. Then the function $\bar{u} \in L^\infty(0,T;H_0^1(\Omega))$, such that $u_{\mathcal{D}_m,\tau_m} \to \bar{u}$ in $L^\infty(0,T;L^2(\Omega))$, is a weak solution of (6)-(2)-(3) in the sense of Definition 1.1. Moreover, $\widehat{G}_{\mathcal{D}_m,\tau_m} \to \nabla\bar{u}$ in $L^2(\Omega\times(0,T))^d$ and $N_{\mathcal{D}_m,\tau_m} \to |\nabla\bar{u}|$ in $L^2(\Omega\times(0,T))$.*

3 Numerical experiments

The goal of this section is to compare both schemes CVS and EHM, first in computing the experimental order of convergence and then on image filtering examples. In the later case we present also results of classical finite difference scheme [10] in order to see superior behavior of our finite volume methods.

3.1 Experiments with exact solution

In the following examples we consider the square domain $\Omega = [-1.25, 1.25] \times [-1.25, 1.25]$. The number of finite volumes along each boundary side is denoted by n, which means that n^2 is the total number of finite volumes. Then $h = 2.5/n$ is the length of the side of each square finite volume and in all experiments time step is equal $\tau = h^2$ and $a = h,\ b$ is large constant.
The numerical solution of the finite volume schemes is obtained through the resolution of linear algebraic system at every discrete time step, we used the Successive Over Relaxation (SOR) iterative solver. Typically, about 30-35 SOR iterations inside semi-implicit scheme in each time step are needed for obtaining the results presented in this section.
In the tables below we compare the results obtained by CVS and EHM schemes. The considered errors are $E_2 = \|u_{\mathcal{D},\tau} - u\|_{L^2(\Omega\times(0,T))}$, $EG_2 = \|\widehat{G}_{\mathcal{D},\tau} - \nabla u\|_{L^2(\Omega\times(0,T))^2}$ and we also report CPU times in seconds.

Example 1. In this example, the exact solution is a paraboloid moving up in time, given by $u(x, y, t) = \frac{1}{2}(x^2 + y^2 - 1) + t$, which is the solution to (1)-(2) where (3) is replaced by the exact non-homogeneous Dirichlet boundary conditions provided by the solution. We consider the time interval $[0, T] = [0, 0.3125]$. In Table 1 we can observe the results obtained by CVS scheme (top) and the results obtained by EHM scheme (bottom) . As one can see , the experimental order of convergence (EOC) in the solution error is equal 2. For the gradient, the EOC for the EHM scheme is higher and also the errors for this scheme are lower on the same time-space grid. On the contrary the CPU time is slightly faster for the CVS scheme.

n	τ	E_2	EOC	EG_2	EOC	CPU
10	6.25e-2	4.00e-2	-	1.25e-1	-	0.0
20	1.5625e-2	1.09e-2	1.87	6.20e-2	1.01	0.0
40	3.90625e-3	2.56e-3	2.10	2.95e-2	1.01	1.0
80	9.76563e-4	6.18e-4	2.05	1.43e-2	1.04	8.0
160	2.44141e-4	1.52e-4	2.02	7.08e-3	1.02	135
320	6.10352e-5	3.78e-5	2.01	3.53e-3	1.01	1582

n	τ	E_2	EOC	EG_2	EOC	CPU
10	6.25e-2	3.51e-2	-	7.82e-02	-	0.
20	1.5625e-2	9.29e-3	1.91	3.13e-2	1.32	0.
40	3.90625e-3	2.12e-3	2.14	9.88e-3	1.66	0.
80	9.76563e-4	5.00e-4	2.08	2.84e-3	1.80	10.0
160	2.44141e-4	1.22e-4	2.04	7.87e-4	1.85	164
320	6.10352e-5	3.01e-5	2.02	2.13e-4	1.88	2064

Table 1: Example 1, error reports, EOCs and CPU times for CVS scheme (top) and EHM scheme (bottom)

Example 2. In this example, the exact viscosity solution of (1) is a truncated paraboloid shrinking in time, given by $u(x, y, t) = \min\{\frac{1}{2}(x^2 + y^2 - 1) + t, 0\}$ [9]. The initial condition and exact solution at time $T = 0.3125$ are plotted in Figure 2.
Numerical results, for $n = 160$, $T = 0.3125$, obtained by both schemes are plotted in Figure 3. Since the gradient of the solution is discontinuous along a shrinking circle, a second order accuracy cannot be

expected in this case. One can see the results for both schemes in Table 2 and behavior of both schemes is similar to Example 1.

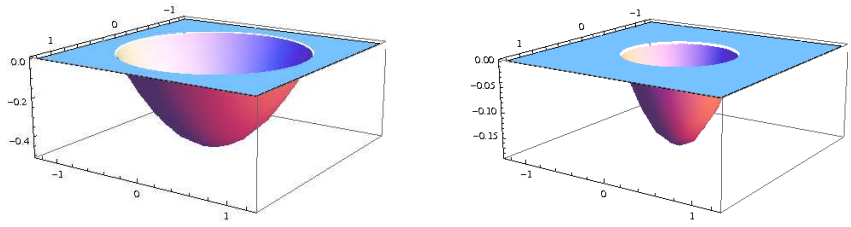

Figure 2: Example 2, the initial condition (left) and exact solution at time T=0.3125

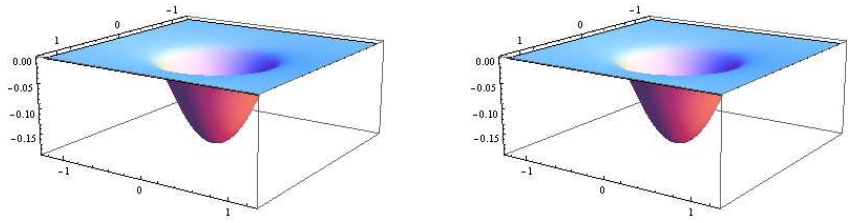

Figure 3: Example 2, CVS scheme (left) and EHM scheme at time T=0.3125

n	τ	E_2	EOC	EG_2	EOC	CPU
10	6.25e-2	6.30e-2	-	2.85e-1	-	0.0
20	1.5625e-2	4.71e-2	0.43	2.41e-1	0.24	0.0
40	3.90625e-3	2.88e-2	0.71	1.89e-1	0.35	1.0
80	9.76563e-4	1.59e-2	0.85	1.49e-1	0.34	8.0
160	2.44141e-4	8.46e-3	0.91	1.18e-1	0.33	137
320	6.10352e-5	4.39e-3	0.95	9.54e-2	0.31	1668
n	τ	E_2	EOC	EG_2	EOC	CPU
10	6.25e-2	6.47e-2	-	2.83e-1	-	0.
20	1.5625e-2	4.77e-2	0.44	2.36e-1	0.26	0.
40	3.90625e-3	2.87e-2	0.73	1.83e-1	0.37	1.
80	9.76563e-4	1.58e-2	0.86	1.43e-1	0.36	10.0
160	2.44141e-4	8.33e-3	0.92	1.11e-1	0.36	166
320	6.10352e-5	4.29e-3	0.96	8.72e-2	0.36	2084

Table 2: Example 2, error reports, EOCs and CPU times for CVS scheme (top) and EHM scheme (bottom)

3.2 Image processing examples

We now turn to the comparison of the schemes in the framework of image processing applications. It is known that mean curvature flow models are suitable for filtering of salt & pepper noise due to curvature blow-up phenomenon and infinite speed of shrinking before the extinction of an object.
As a $2D$ image can be represented as a piecewise constant function of the gray level intensity in each pixel, we prescribe the initial condition only in the representative points x_p of each finite volume. We

denote these values u_p^0 and we approximate the values at the points x_σ on each edge by a median of six neighbouring pixel values and denote them by u_σ^0 in EHM scheme and u_m^0 in CVS scheme. Moreover, the values u_r^0 in CVS scheme we compute as a median of four neighbouring pixel values.
We choose the relation $\tau = h$ for image processing exmaples with $h = 0.1$ and $n = 400$. For solving linear algebraic system of equations we use SOR iterative method with relaxation parameter $\omega = 1.6$. We need approximately 60 iterative steps to obtain the results with residuum tolerance 10^{-10}.

Example 3. In this example we add 20 percent salt & pepper noise to the characteristic function of a cinquefoil, and we set $n = 400$. Figures 4 and 5 show almost perfect cinquefoil reconstruction using both schemes, the result was obtained after 10 time steps of EHM and CVS schemes.

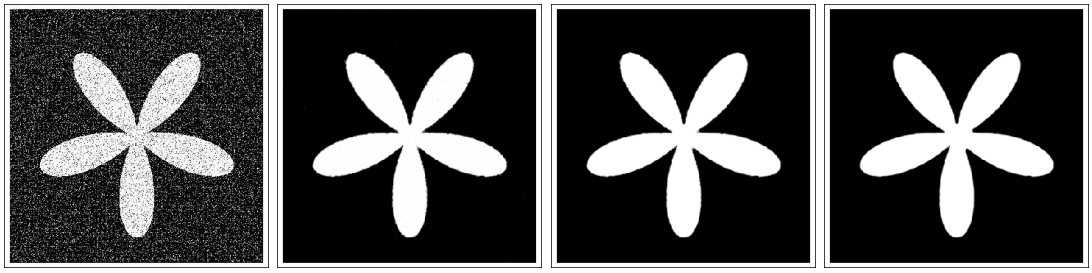

Figure 4: Example 3, EHM scheme: initial noisy image with 20 percent salt & pepper noise added (left), filtering results after 1 (middle) and 3 (right) and 10 time steps (extreme right).

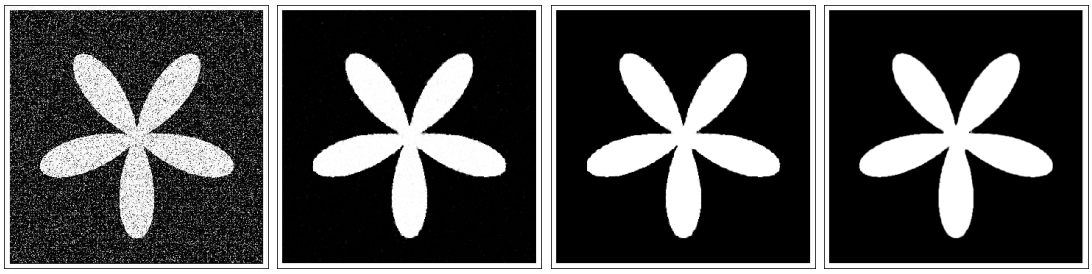

Figure 5: Example 3, CVS scheme: initial noisy image with 20 percent salt & pepper noise added (extreme left), filtering results after 1 (middle left), 4 (middle right), and 10 (extreme right) time steps.

Example 4. In the last example we add strong 50 percent salt & pepper noise to the characteristic function of the quatrefoil. Figures 6 and 7 show again very good quatrefoil reconstruction using EHM and CVS scheme respectively after just few time steps. In Figure 8, for comparison, we show that with such high level of noise reconstruction of quatrefoil using classical finite difference scheme [10] fails.

4 Conclusion and future work

Two different semi-implicit numerical schemes based on the finite volume method for approximation of the regularised mean curvature flow level set equation were investigated. The first, CVS scheme, is based on co-volume strategy and nonlinear terms, given by the absolute value of gradient, are evaluated on pixel sides using splitted diamond-cell approach [11, 7, 8, 2, 6]. In the second, EHM scheme, the absolute values of gradients are evlauated inside the pixels by the Stokes formula and the scheme is obtained by imposing the continuity of fluxes on pixel sides [4]. Results concerning numerical analysis of the schemes

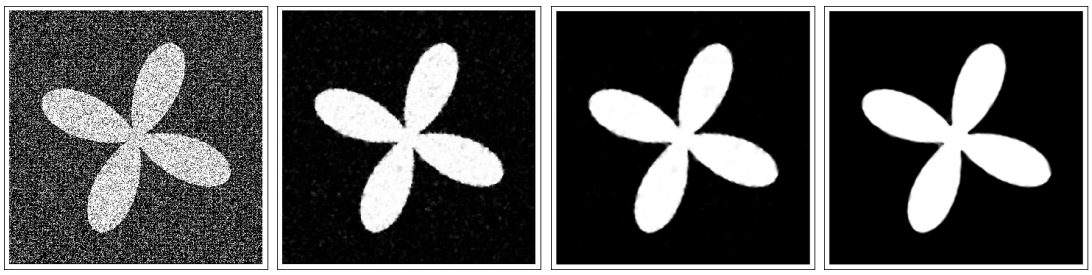

Figure 6: Example 4, EHM scheme: initial noisy image with 50 percent salt & pepper noise added (extreme left), filtering result after 1 (middle left), 3 (middle right) and 10 (extreme right) time steps.

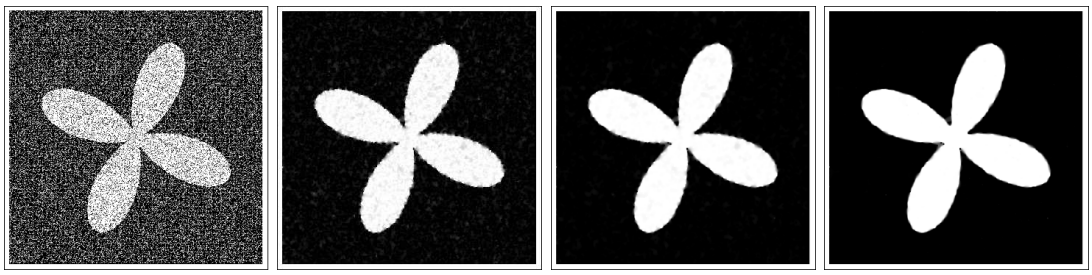

Figure 7: Example 4, CVS scheme: initial noisy image with 50 percent salt & pepper noise added (extreme left), filtering result after 1 (middle left), 3 (middle right) and 10 (extreme right) time steps.

were presented and a comparison of these numerical approximations on several representative examples were discussed including performance in image filtering.
Both schemes can be modified to a numerical aproximation of the generalized equations like the geodesic mean curvature flow (arising e.g. in image segmentation) by the generalized subjective surface method [2, 8] which will be an objective of our further study.

Acknowledgement. The work of A.H., K.M. was supported by the grants APVV-0184-10 and VEGA 1/0269/09.

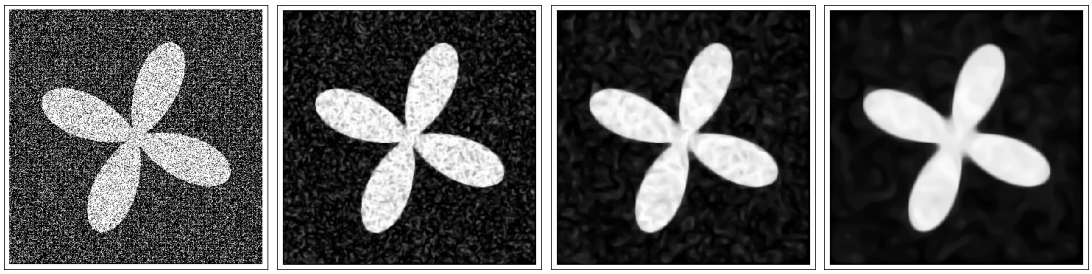

Figure 8: Example 4, explicit finite difference scheme: initial noisy image with 50 percent salt & pepper noise added (extreme left), filtering result after 10 (middle left), 50 (middle right) and 200 (extreme right) time steps, here due to stability constrain $\tau = h^2/4$.

References

[1] G. Barles, P.E.Souganidis, *Convergence of approximation schemes for fully nonlinear second order equations,* Asymptotic Analysis 4: 271–283, 1991.

[2] S. Corsaro, K. Mikula, A. Sarti, F. Sgallari, *Semi-implicit co-volume method in 3D image segmentation,* SIAM Journal on Scientific Computing, 28 (6):2248-2265, 2006.

[3] R. Eymard T. Gallouët and R. Herbin, *Finite volume methods.* Ciarlet, P. G. (ed.) et al., Handbook of numerical analysis. Vol. 7: Solution of equations in $\mathbb{R}^n$ (Part 3). Techniques of scientific computing (Part 3). Amsterdam: North-Holland/ Elsevier,: 713-1020, 2000.

[4] R. Eymard, A. Handlovičová and K. Mikula, *Study of a finite volume scheme for the regularized mean curvature level set equation,* IMA J Numer Anal, 31 (3): 813–846, 2011.

[5] L.C. Evans and J. Spruck, *Motion of level sets by mean curvature I,* J. Differ. Geom., 33(3): 635–681, 1991.

[6] A. Handlovičová, K. Mikula, *Stability and consistency of the semiimplicit co-volume scheme for regularized mean curvature flow equation in level set formulation,* Applications of Mathematics, 2: 105–129, 2008.

[7] A. Handlovičová, K. Mikula, F. Sgallari, *Semi-implicit complementary volume scheme for solving level set like equations in image processing and curve evolution,* Numer. Math., 93: 675–695, 2003.

[8] K. Mikula, A. Sarti, F. Sgallari, *Co-volume level set method in subjective surface based medical image segmentation,* Handbook of Medical Image Analysis: Segmentation and Registration Models J.Suri et al., Eds., Springer, New York, 583–626, 2005.

[9] A. M. Oberman, *A convergent monotone difference scheme for motion of level sets by mean curvature,* Numer. Math., 99 (2):365–379. 2004.

[10] S. Osher, J. Sethian, *Fronts propagating with curvature dependent speed: algorithm based on Hamilton-Jacobi formulation,* J.Comput. Phys., 79:12–49, 1988.

[11] N. J. Walkington, *Algorithms for computing motion by mean curvature,* SIAM J. Numer. Anal., 33 (6): 2215–2238, 2006.